

## MIT Open Access Articles

*Electric field measurements of DC-driven positive streamer coronas using the E-FISH method*

The MIT Faculty has made this article openly available. **Please share** how this access benefits you. Your story matters.

**Citation:** Strobel, Lee R., Martell, Benjamin C., Morozov, Anatoli, Dogariu, Arthur and Guerra-Garcia, Carmen. 2022. "Electric field measurements of DC-driven positive streamer coronas using the E-FISH method." 121 (11).

**As Published:** 10.1063/5.0100941

**Publisher:** AIP Publishing

**Persistent URL:** <https://hdl.handle.net/1721.1/145521>

**Version:** Final published version: final published article, as it appeared in a journal, conference proceedings, or other formally published context

**Terms of use:** Creative Commons Attribution 4.0 International license



# Electric field measurements of DC-driven positive streamer coronas using the E-FISH method

Cite as: Appl. Phys. Lett. **121**, 114102 (2022); <https://doi.org/10.1063/5.0100941>

Submitted: 27 May 2022 • Accepted: 20 August 2022 • Published Online: 15 September 2022

Published open access through an agreement with Massachusetts Institute of Technology

 Lee R. Strobel,  Benjamin C. Martell,  Anatoli Morozov, et al.



View Online



Export Citation



CrossMark

## ARTICLES YOU MAY BE INTERESTED IN

[High-pressure structural stability and bandgap engineering of layered tin disulfide](#)

Applied Physics Letters **121**, 114101 (2022); <https://doi.org/10.1063/5.0107303>

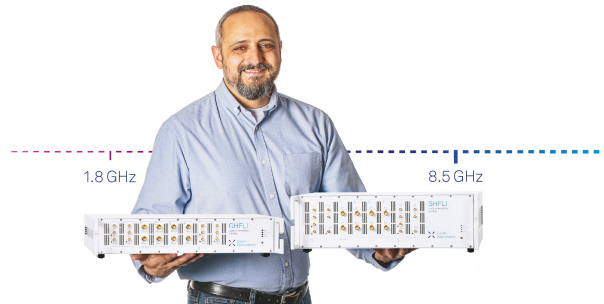
[Native defect-related broadband ultrafast photocarrier dynamics in n-type  \$\beta\$ -Ga<sub>2</sub>O<sub>3</sub>](#)

Applied Physics Letters **121**, 112103 (2022); <https://doi.org/10.1063/5.0100190>

[Giant power density from BiFeO<sub>3</sub>-based ferroelectric ceramics by shock compression](#)


Applied Physics Letters **121**, 113903 (2022); <https://doi.org/10.1063/5.0102102>





**Trailblazers.** New

Meet the Lock-in Amplifiers that measure microwaves.

 Zurich Instruments

[Find out more](#)

# Electric field measurements of DC-driven positive streamer coronas using the E-FISH method

Cite as: Appl. Phys. Lett. **121**, 114102 (2022); doi: [10.1063/5.0100941](https://doi.org/10.1063/5.0100941)

Submitted: 27 May 2022 · Accepted: 20 August 2022 ·

Published Online: 15 September 2022



View Online



Export Citation



CrossMark

Lee R. Strobel,<sup>1,a)</sup> Benjamin C. Martell,<sup>1</sup> Anatoli Morozov,<sup>2</sup> Arthur Dogariu,<sup>2,3</sup> and Carmen Guerra-García<sup>1,a)</sup>

## AFFILIATIONS

<sup>1</sup>Department of Aeronautics and Astronautics, Massachusetts Institute of Technology, Cambridge, Massachusetts 02139, USA

<sup>2</sup>Department of Mechanical and Aerospace Engineering, Princeton University, Princeton, New Jersey 08544, USA

<sup>3</sup>Department of Aerospace Engineering, Texas A&M University, College Station, Texas 77843, USA

<sup>a)</sup>Authors to whom correspondence should be addressed: [lstrobel@mit.edu](mailto:lstrobel@mit.edu) and [guerrac@mit.edu](mailto:guerrac@mit.edu)

## ABSTRACT

This paper reports on electric field measurements, using the electric field-induced second harmonic (E-FISH) method, sampling the spatial structure and temporal development of DC-driven positive streamer coronas in atmospheric-pressure air at relevant timescales to examine the self-pulsating behavior of the discharge. The discharge is triggered from a point-to-plate geometry and consists of transient coronas, which bridge the inter-electrode gap and pulsate at about 3 kHz, superimposed with a persisting glow corona. The measurements presented challenge the phenomenological explanation for the pulsations based on field recovery at the anode driven by the evacuation of positive ions by electric drift effects and hint at a propagating wave-like feature from the plate-cathode to the tip-anode.

© 2022 Author(s). All article content, except where otherwise noted, is licensed under a Creative Commons Attribution (CC BY) license (<http://creativecommons.org/licenses/by/4.0/>). <https://doi.org/10.1063/5.0100941>

Impulsive coronas, driven by DC voltage, can be traced back to the classical works of Loeb and his school.<sup>1,2</sup> The most simple setup considers a point-to-plate geometry, with small radius of curvature ( $\sim 100\ \mu\text{m}$ ) and small gap distances ( $\sim 1\ \text{cm}$ ) in atmospheric air. Despite the DC voltage, the discharge is a superposition of a localized glow corona, characterized by electrical and visual stability, and impulsive discharges or streamer coronas, which develop with good reproducibility in space and time at high repetition rates (1–10 kHz in the positive polarity).<sup>2</sup> These streamer coronas are tree-like structures, comprised of thin filaments of nonthermal plasma, which propagate from the high-voltage electrode.

Self-pulsating discharges under DC or ramped voltage ( $\sim \text{kV}/\mu\text{s}$ ) are of relevance in atmospheric electricity studies, e.g., self-pulsating streamer coronas are often used as indicators of imminent leader formation<sup>3</sup> and also appear in transmission lines.<sup>4</sup> DC-driven self-oscillatory discharges, in point-to-plate configurations<sup>5,6</sup> and atmospheric pressure plasma jets,<sup>7</sup> have also been proposed as inexpensive sources of nonthermal plasma for use in the fields of bio-engineering, food processing, medicine, and more.<sup>5,8–11</sup>

The underlying physics of the impulsive corona is similar to those encountered in pulsed-voltage discharges (with applied voltage pulses of tens to hundreds of nanosecond duration<sup>12,13</sup>) with typically far fewer streamers and less branching observed. Unique to the DC case is

the self-pulsating mechanism, which is generally explained in terms of charge accumulation effects in the vicinity of the stressed electrode;<sup>14,15</sup> i.e., the ionic space charge that forms during an impulsive corona locally reduces the electric field, suppressing the discharge until this space charge drifts away.<sup>15</sup> This phenomenological description is widely accepted but has not been confirmed experimentally.

Recently, the Electric Field-Induced Second Harmonic generation (E-FISH) method has been developed as a noninvasive diagnostic technique<sup>16</sup> that is able to make direct measurements of the electric field in any gas mixture or plasma, with sub-nanosecond resolution in time and tens of micrometers resolution in space.<sup>17</sup> This technique exploits a nonlinear optical phenomenon, whereby in the presence of an electric field, two photons of a high-power laser interact with the medium to generate a photon that has double the frequency, with the intensity of the second harmonic beam having a quadratic dependency on the electric field strength. Prior to this, direct measurements of the electric field inside streamer coronas were not feasible: a physical probe would disrupt the discharge, and other noncontact techniques were more restrictive in pressure and gas composition.<sup>18–20</sup>

In this work, direct measurements of the time-evolution of the electric field inside DC-driven positive streamer coronas in atmospheric-pressure air, during the period between two consecutive pulses, using the E-FISH technique, are presented. Measurements are

taken at several vertical locations within the discharge gap, to quantitatively determine the mechanisms driving the pulsations. Prior studies<sup>21–23</sup> have used E-FISH to investigate other types of discharges, but none have focused on self-pulsating streamer coronas.

Representative DC streamer coronas studied in this work are shown in Fig. 1(a). The coronas initiate from a tungsten tip-anode and propagate toward a grounded aluminum plate 25 mm from it. The discharge is initiated using a Matsusada RB60-30 DC high voltage power supply. For the experiments presented, the DC level is set to 14 kV, unless otherwise indicated. Figure 1(a) shows the different measurement locations selected to sample the corona structure: capturing the vicinity of the tip, the stem of the discharge, and the branching region. The experimental setup is shown in Fig. 1(b). The optical circuit is similar to that described by Goldberg *et al.*,<sup>17</sup> and the reader is referred to that publication for details. The beam from a Spectra-Physics Solstice Ace femtosecond laser (800 nm) is focused into a laser sheet using an  $f = 0.4$  m cylindrical lens, to give a one-dimensional measurement of the electric field at a given vertical position, with a FWHM of 4.8 mm. The second harmonic beam is routed to a Princeton Instruments PI-MAX4 ICCD camera. The current waveform is

measured using a shunt resistor. A digital delay generator is used for synchronization, and all signals are recorded using a digital oscilloscope.

The electric field measurements were calibrated using two flat plates spaced 30 mm apart, and with an applied voltage varying from 0 to 30 kV, in 5 kV increments. The luminosity measured by the camera sensor (capturing the second harmonic beam) was integrated vertically to give a 1D signal. The quadratic dependency with the electric field strength was used to obtain fit coefficients for each individual horizontal camera pixel, correlating luminosity to electric field magnitude. Particular to these experiments are the timing and synchronization schemes used, since the discharges are self-pulsating [Fig. 1(c)] with significant dispersion in the inter-pulse period, e.g.,  $333 \pm 5.8$   $\mu$ s (mean  $\pm$  standard deviation) in the example shown. Time-resolved E-FISH measurements were taken at two different timescales relative to the discharge current pulse: a shorter ns timescale during and just after the current pulse and a longer  $\mu$ s timescale, spanning the period between two successive discharge pulses.

Figure 1(d) shows the synchronization scheme used. The camera trigger pulse was set to variable delays relative to the laser pulse.

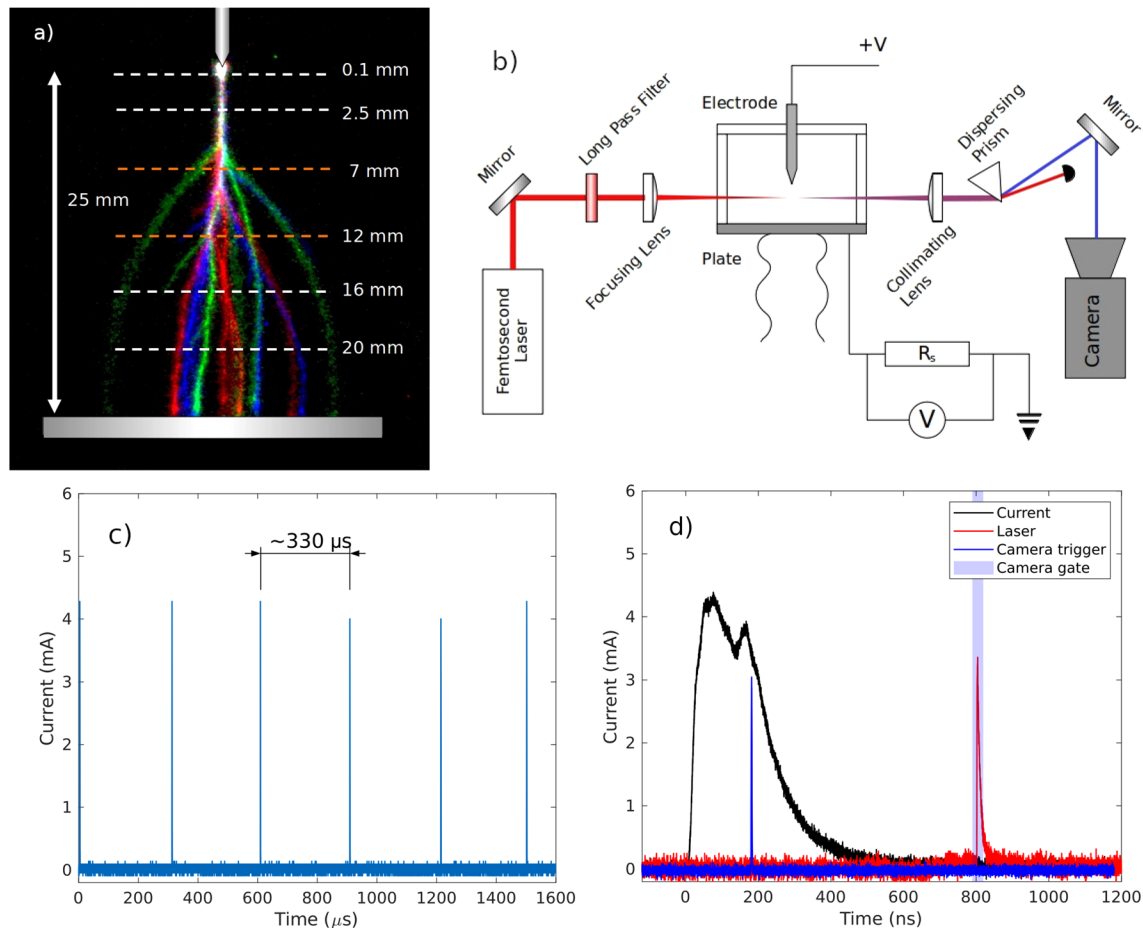


**FIG. 1.** Experimental setup and timing schemes. (a) Intensified charge-coupled device (ICCD) images of three overlaid independent streamer bursts, with the E-FISH measurement positions indicated by dashed lines. (b) Simplified schematic of the experimental setup. (c) Train of six successive discharges, showing the pulsating behavior. (d) Timing and synchronization scheme for data taken immediately after a burst, using the coincidence of the camera trigger (blue) and the current pulse (black).

The laser timing relative to the discharge was ensured by only triggering the camera upon a coincidence of the current pulse and camera trigger pulse. This introduced some random delay comparable to the pulse width  $\sim 350$  ns. The camera gate width was set to 30 ns and timed, so that it always coincided with the laser. The acquired images were then aligned relative to the start of the current pulse. This scheme allows sampling of the decay region of the current pulse, but not the sharp rise of the current as there is a minimum delay of  $\sim 120$  ns between the camera trigger and the time when the image is taken (accounting for optical and electrical paths). For the short timescales, sets of images were taken with delays between the camera trigger and laser of 120–2220 ns in 300 ns increments. Individual images were then binned according to the actual measured delay time from the start of the current pulse, such that there were at least 200 images per bin.

Longer timescale measurements were taken to probe the behavior of the electric field over the inter-pulse period. For the results in Figs. 2(b), 3(b) and 5, a single measurement was taken at each time point comprising 200 image accumulations on the camera sensor. The timing between the current pulse and laser was adjusted as before, and measurements were taken at 2, 5, 10, 20, 30, 40, and 50  $\mu$ s and then every 25  $\mu$ s up to 350  $\mu$ s, to cover the full inter-pulse period. For the results presented in Fig. 4, two additional vertical positions were measured, and the measurements at 2.5 mm were taken at finer spacings of 10  $\mu$ s, to provide better clarity on the field behavior ahead of the next pulse. In this case, individual frames were captured rather than accumulated images, with the timing of the following pulse captured for each sample. This allowed measurements to be filtered, based on whether they were before or after the subsequent pulse.

The estimated random error is indicated as shaded regions (Figs. 3 and 4), which is the standard error of all the image samples for each data point. Given the large sampling and spatial averaging, the random error is small. Note that there are other sources of systematic error that are not displayed, mostly related to the dependence of the E-FISH signal on the spatial profile of the external field, which is unknown *a priori* in a plasma as well as the calibration method performed, which does not account for spatial nonuniformity effects. Chng *et al.* have published a series of papers<sup>24,25</sup> discussing the inaccuracies in absolute electric field determination when using the E-FISH technique with focused beams.<sup>26</sup> Note that the key findings and conclusions presented here are based on the relative shapes of the time-varying electric field curves (Figs. 3–5) and not so much on the magnitude of the fields measured. Most of the figures are, however, displayed in dimensional units for future repeatability of the results.

Figure 2 shows plots of the spatial electric field measured for (a) the short timescales and (b) the long timescales. The x-axis represents the horizontal position along the laser line (parallel to the ground plate). The left-hand y-axis shows the location of the laser sheet relative to the tip. The right-hand y-axis of each subplot shows the magnitude of the electric field in kV/cm. Each sub-plot shows electric field curves for a range of time values. For reference, the electric field in the absence of space charge, calculated using a Hybridizable Discontinuous Galerkin (HDG) numerical model,<sup>27</sup> is shown.

The spatial structure of the discharge observed in the electric field measurements (Fig. 2) is consistent with its visual structure [Fig. 1(a)]: with strongly nonuniform profiles for the two locations closest to the tip and mostly uniform profiles for the locations closest to the plate. It is interesting to note the different behavior of the measurements at 0.1

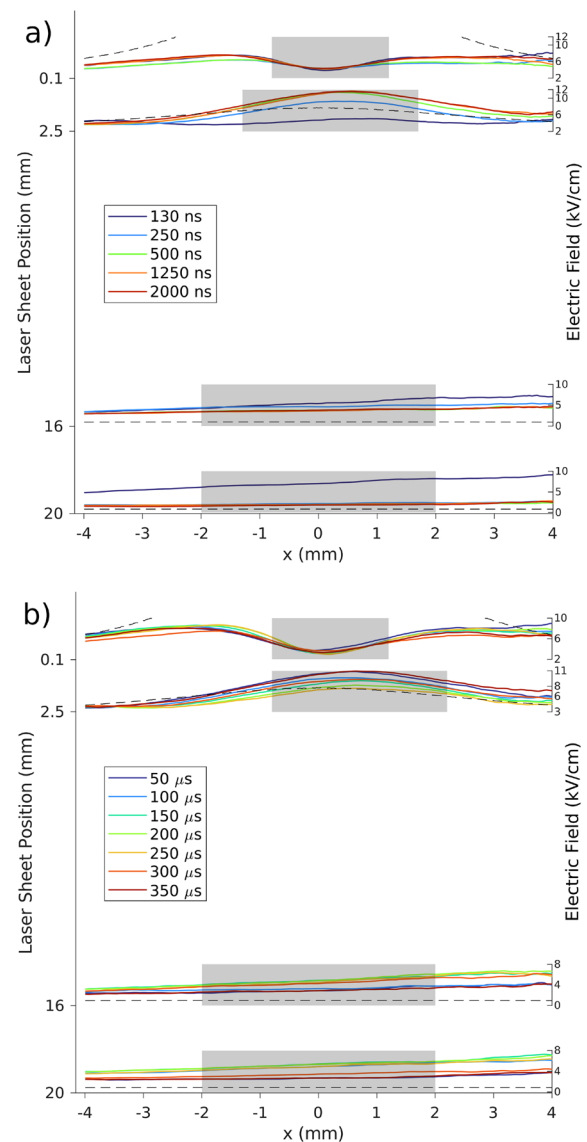


**FIG. 2.** 1D spatial electric field measurements, with time as a parameter. (a) Short timescales (ns) and (b) long timescales ( $\mu$ s). Dashed black lines show the results of an HDG numerical model for the Laplacian field.

and 2.5 mm, with the electric field profile at 0.1 mm showing a clear dip in the field at approximately the location of the anode, and the field at 2.5 mm not presenting this feature. Whereas an enhancement of the field aligned with the anode is to be expected for the Laplacian solution, due to the small radius of curvature of the tip, the dip close to the electrode seems to indicate the presence of strong space charge shielding, which persists for the duration of the inter-pulse period and possibly is related to the underlying glow. The measurement at 2.5 mm captures the stem of the discharge and does not display a dip, which could be due to a number of reasons, such as averaging over multiple bursts that are not perfectly aligned or the characteristic size of the shielding region being comparable to the region of influence of



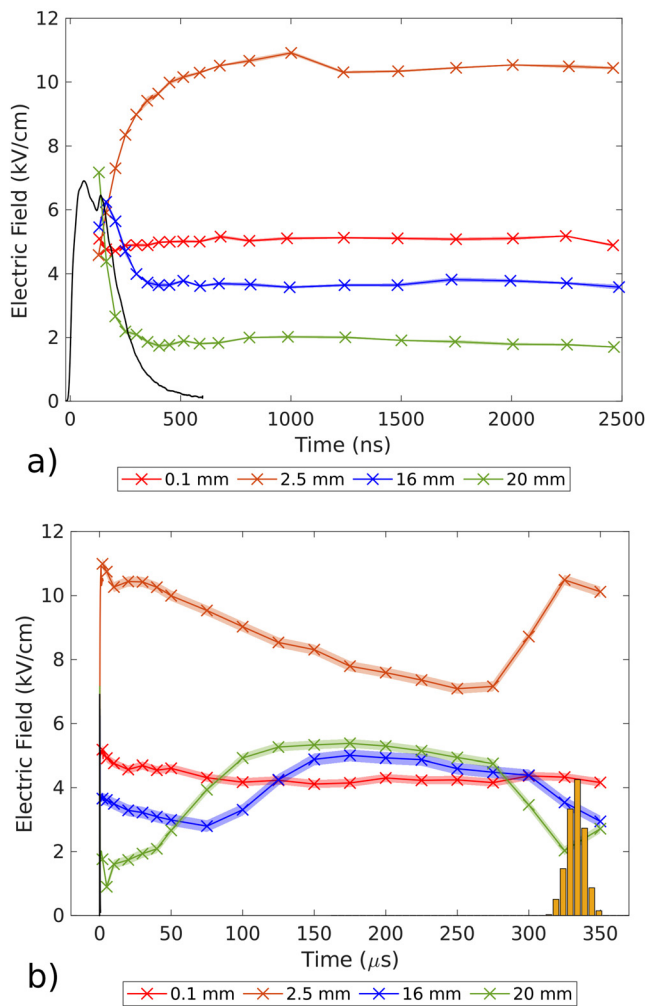


**FIG. 3.** Spatially averaged electric field (using the bins shown in Fig. 2) as a function of time. (a) Short ns timescales, with current pulse plotted in black. (b) Long  $\mu$ s timescales, with timing histogram for the subsequent pulse.

the sharp electrode at that location. The results of the two measurements in the branching region (at 16 and 20 mm) are fairly uniform, which is to be expected, as the branching pattern of each corona is different [Fig. 1(a)] and  $>200$  coronas are being averaged. The nonuniformity in  $x$  may be due to a horizontal shift in the calibration curve, due to misalignment of the camera. This would cause the predicted field to be too low on one side and too high on the other.

To further explore the time-evolution of the electric field, Fig. 3 shows spatially averaged plots of the electric field for (a) the short timescales and (b) the longer timescales. The range of spatial averaging is shown as the gray shaded areas in Fig. 2, chosen to focus on the dips/peaks that are apparent in the profiles. A histogram of the timing of the subsequent pulses is shown in yellow. After the current rise, and for the closest sampling times accessible with the proposed timing scheme [Fig. 3(a)], the spatially averaged electric field curves for the four measurement positions seem to converge to approximately the same value. As the discharge bridges the gap and a higher current is

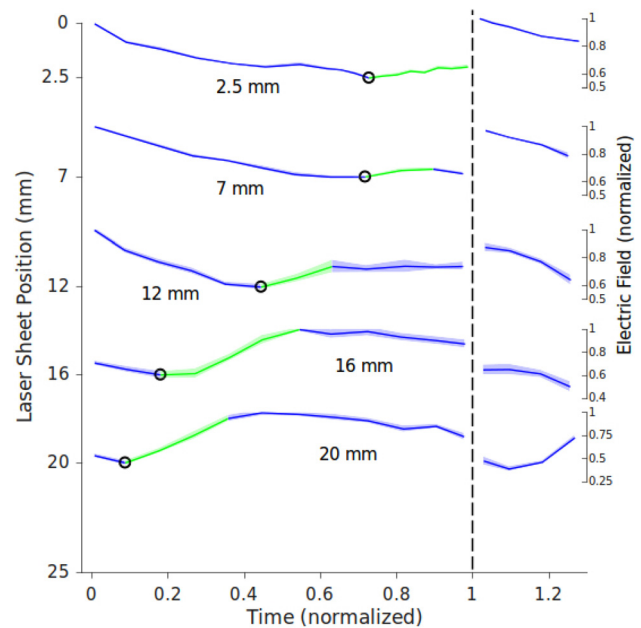


**FIG. 4.** Spatially averaged electric field as a function of time for long  $\mu$ s timescales, separating the vertical measurements to reveal traveling features. Electric field and time are normalized by the maximum field at that location and the time period to the next discharge, respectively.

flowing, the field equalizes, and the measured value is consistent with the expected average field (the applied potential of 14 kV divided by the gap size of 25 mm). During the decay time of the current pulse (of order  $\sim 250$  ns), the electric fields at the separate locations rapidly evolve to different fairly steady levels that persist for the next 2  $\mu$ s. The recovery of the fields following the convergence is very fast,  $<500$  ns, indicating that the behavior is driven by the electrons. This behavior is consistent with prior observations.<sup>6,14,28</sup>

At the longer timescales [Fig. 3(b)], some unexpected behavior can be seen. None of the positions displays a monotonically increasing field that would correspond to the classical explanation for the self-pulsating behavior being driven by removal of residual space charge. The uppermost position (0.1 mm) seems to stay relatively constant for the whole inter-pulse duration (also true for the short timescales), which may relate to the persistent presence of the glow corona. The field at the 2.5 mm position significantly decreases, from the value of  $\sim 10$  kV/cm that it settled at after the current pulse, over most of the inter-pulse period. The field increase observed over the final  $\sim 50$   $\mu$ s can be mostly attributed to the triggering of the following pulse, spread out in time due to the dispersion in the event. For the lower positions within the branching region (16 and 20 mm), the results show the spatially averaged electric field rising up to maintain a roughly steady level between about 150 and 275  $\mu$ s.

Figure 4 plots similar data to Fig. 3(b), but laid out separating the vertical measurements, to help visualize any traveling features. The data were taken using a different anode-needle at 17 kV, and results are normalized in time by the corresponding inter-pulse period. The shapes of the curves are consistent with those shown in Fig. 3(b), and the behavior of the field following the next pulse is consistent with the

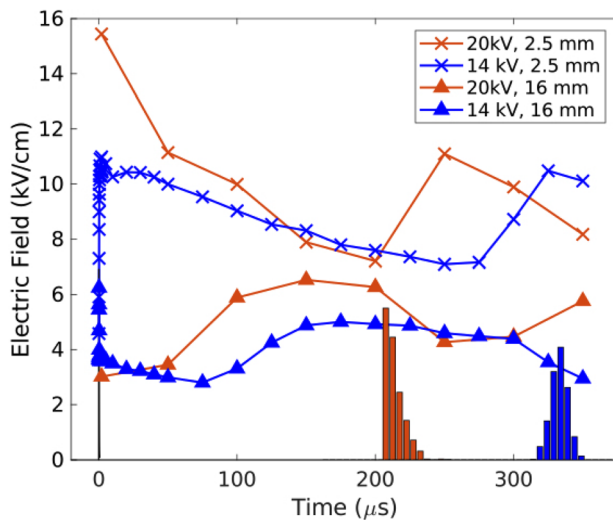


**FIG. 5.** Spatially averaged electric field vs time, comparing cases with different applied voltages. Results and pulse histograms shown in blue for 14 kV and orange for 20 kV.

behavior following the triggering pulse at time = 0. Note that small differences between the 0–0.2 range and the 1–1.2 range can be attributed to a smaller number of samples in the 1–1.2 range (larger error bars). A clear jump is observed in the field at all locations after the next discharge strikes, consistent with Fig. 3(a). The field at 2.5 mm appears to rise a little ahead of the next pulse; however, the following pulse is not being triggered at a maximum of the electric field, which indicates the onset of the next pulse is not primarily being caused by field recovery. An increase in the field (highlighted in green) is observed at all locations, which appears to start later for higher positions in the discharge gap. This indicates the presence of a wave propagating from the lower positions up toward the anode, with a speed  $\sim 80$  m/s. This speed is comparable to that of the ion drift in the measured fields: e.g., using an ion mobility<sup>29</sup> of  $\mu \sim 1.4$  cm<sup>2</sup>/V/s and an average field of 5.6 kV/cm, which suggests it may be linked to ionic effects.

The effect of increasing the applied voltage is illustrated in Fig. 5. The spatially averaged electric field measurements show similar temporal features for different applied voltages, but the electric field evolves more quickly for higher voltage, suggesting the role of electrostatic effects. The curves overlap quite closely when normalized in time by the mean inter-pulse period. Overall, the average fields are higher for higher applied voltage.

In conclusion, direct measurements of the electric field inside a self-pulsating positive DC streamer corona have been presented, both spatially and time-resolved, using the recently developed E-FISH diagnostic technique. The results are surprising in several ways and seem to challenge the conventional theory that the timing of a self-pulsating positive streamer corona is driven by field recovery at the anode, due to the evacuation of positive ions by the electric field. The results suggest that the self-pulsation frequency may relate to the propagation of a wave from the cathode toward the anode, driven by ionic processes. The nature of this wave is unknown and prompts fundamental questions that will be addressed in future work.

This research used resources of the Princeton Collaborative Low Temperature Plasma Research Facility, PCRF (<http://pcrf.pppl.gov>), a collaborative research facility supported by the U.S. Department of Energy, Office of Science, Office of Fusion Energy Sciences under Contract No. DE-AC02-09CH11466. The MIT team acknowledges partial support by The Boeing Company through the Strategic Universities for Boeing Research and Technology Program. L. Strobel acknowledges support through a Mathworks fellowship.

## AUTHOR DECLARATIONS

### Conflict of Interest

The authors have no conflicts to disclose.

### Author Contributions

**Lee Richard Strobel:** Data curation (lead); Formal analysis (lead); Investigation (equal); Methodology (equal); Software (lead); Visualization (lead); Writing – original draft (lead); Writing – review & editing (equal). **Benjamin C. Martell:** Data curation (supporting); Investigation (equal); Methodology (equal); Writing – review & editing (supporting). **Anatoli V. Morozov:** Investigation (supporting); Methodology (supporting); Resources (equal); Writing – review & editing (supporting). **Arthur Dogariu:** Conceptualization (equal); Data curation (supporting); Funding acquisition (lead); Investigation (equal); Methodology (equal); Resources (equal); Supervision (equal); Visualization (supporting); Writing – review & editing (supporting). **Carmen Guerra-Garcia:** Conceptualization (lead); Data curation (supporting); Formal analysis (equal); Funding acquisition (lead); Investigation (equal); Methodology (equal); Project administration (lead); Resources (equal); Supervision (lead); Visualization (equal); Writing – original draft (lead); Writing – review & editing (equal).

## DATA AVAILABILITY

The data that support the findings of this study are available from the corresponding authors upon reasonable request.

## REFERENCES

- <sup>1</sup>L. B. Loeb, *Electrical Coronas*, 1st ed. (University of California Press, 1965).
- <sup>2</sup>M. Goldman and A. Goldman, “Corona discharges,” in *Gaseous Electronics*, 1st ed. (Academic Press, Inc., 1978), Chap. 4, Vol. 1, pp. 219–285.
- <sup>3</sup>I. Gallimberti, G. Bacchiega, A. Bondiou-Clergerie, and P. Lalande, “Fundamental processes in long air gap discharges,” *C. R. Phys.* **3**, 1335–1359 (2002).
- <sup>4</sup>X.-C. Zhang, F. Wang, N.-N. Liu, A.-Q. Li, and W.-L. Fan, “Particle simulation of streamer discharges on surface of DC transmission line in presence of rain-drops,” *J. Appl. Phys.* **129**, 183306 (2021).
- <sup>5</sup>J. Khun, V. Scholtz, P. Hozák, P. Fitl, and J. Julák, “Various DC-driven point-to-plane discharges as non-thermal plasma sources and their bactericidal effects,” *Plasma Sources Sci. Technol.* **27**, 065002 (2018).
- <sup>6</sup>M. Janda, K. Hensel, and Z. Machala, “Kinetic plasma chemistry model of pulsed transient spark discharge in air coupled with nanosecond time-resolved imaging and spectroscopy,” *J. Phys. D* **51**, 334002 (2018).
- <sup>7</sup>X. Wang and A. Shashurin, “DC-driven plasma gun: Self-oscillatory operation mode of atmospheric-pressure helium plasma jet comprised of repetitive streamer breakdowns,” *Plasma Sources Sci. Technol.* **26**, 02LT02 (2017).
- <sup>8</sup>E. Moreau, P. Audier, and N. Benard, “Ionic wind produced by positive and negative corona discharges in air,” *J. Electrostat.* **93**, 85–96 (2018).

- <sup>9</sup>X. He, Y. Zeng, J. Chen, F. Wang, Y. Fu, F. Feng, and H. Huang, "Role of O<sub>3</sub> in the removal of HCHO using a DC streamer plasma," *J. Phys. D* **52**, 465203 (2019).
- <sup>10</sup>Q. Z. Zhang and A. Bogaerts, "Plasma streamer propagation in structured catalysts," *Plasma Sources Sci. Technol.* **27**, 105013 (2018).
- <sup>11</sup>S. Chen, R. G. W. van den Berg, and S. Nijdam, "The effect of DC voltage polarity on ionic wind in ambient air for cooling purposes," *Plasma Sources Sci. Technol.* **27**, 055021 (2018).
- <sup>12</sup>T. M. P. Briels, J. Kos, G. J. J. Winands, E. M. Van Veldhuizen, and U. Ebert, "Positive and negative streamers in ambient air: Measuring diameter, velocity and dissipated energy," *J. Phys. D* **41**, 234004 (2008).
- <sup>13</sup>S. Nijdam, E. Takahashi, A. H. Markosyan, and U. Ebert, "Investigation of positive streamers by double-pulse experiments, effects of repetition rate and gas mixture," *Plasma Sources Sci. Technol.* **23**, 025008 (2014).
- <sup>14</sup>E. Marode, "The mechanism of spark breakdown in air at atmospheric pressure between a positive point and a plane. I. Experimental: Nature of the streamer track," *J. Appl. Phys.* **46**, 2005–2015 (1975).
- <sup>15</sup>Y. P. Raizer, *Gas Discharge Physics*, 1st ed. (Springer, 1997).
- <sup>16</sup>A. Dogariu, B. M. Goldberg, S. O'Byrne, and R. B. Miles, "Species-independent femtosecond localized electric field measurement," *Phys. Rev. Appl.* **7**, 024024 (2017).
- <sup>17</sup>B. M. Goldberg, S. Reuter, A. Dogariu, and R. B. Miles, "1D time evolving electric field profile measurements with sub-ns resolution using the E-FISH method," *Opt. Lett.* **44**, 3853 (2019).
- <sup>18</sup>B. M. Obradović, S. S. Ivković, and M. M. Kuraica, "Spectroscopic measurement of electric field in dielectric barrier discharge in helium," *Appl. Phys. Lett.* **92**, 191501 (2008).
- <sup>19</sup>P. Böhm, M. Kettlitz, R. Brandenburg, H. Höft, and U. Czarnetzki, "Determination of the electric field strength of filamentary DBDs by CARS-based four-wave mixing," *Plasma Sources Sci. Technol.* **25**, 054002 (2016).
- <sup>20</sup>J. Vaudolon and S. Mazouffre, "Indirect determination of the electric field in plasma discharges using laser-induced fluorescence spectroscopy," *Phys. Plasmas* **21**, 093505 (2014).
- <sup>21</sup>Y. Cui, H. Wang, C. Zhuang, H. Luo, X. Wang, and R. Zeng, "Electric field measurement in dielectric barrier discharges using electric field induced second harmonic generation in ambient air," *IEEE Trans. Dielectr. Electr. Insul.* **27**, 2071–2077 (2020).
- <sup>22</sup>K. Orr, Y. Tang, M. Simeni Simeni, D. van den Bekerom, and I. V. Adamovich, "Measurements of electric field in an atmospheric pressure helium plasma jet by the E-FISH method," *Plasma Sources Sci. Technol.* **29**, 035019 (2020).
- <sup>23</sup>Y. Inada, T. Shioda, R. Nakamura, M. Maeyama, A. Kumada, S. Nakamura, and R. Ono, "Systematic 1D electric field induced second harmonic measurement on primary-to-secondary transition phase of positive streamer discharge in atmospheric-pressure air," *J. Phys. D* **55**, 385201 (2022).
- <sup>24</sup>T. L. Chng, S. M. Starikovskaia, and M.-C. Schanne-Klein, "Electric field measurements in plasmas: How focusing strongly distorts the E-FISH signal," *Plasma Sources Sci. Technol.* **29**, 125002 (2020).
- <sup>25</sup>T. L. Chng, D. Z. Pai, O. Guaitella, S. M. Starikovskaia, and A. Bourdon, "Effect of the electric field profile on the accuracy of E-FISH measurements in ionization waves," *Plasma Sources Sci. Technol.* **31**, 015010 (2022).
- <sup>26</sup>The calculated phase mismatch ( $\Delta k$ ) in this case is  $-1.18 \text{ cm}^{-1}$ , giving a phase match (coherence) length of 2.66 cm. This is larger than the expected extent of the discharge field in the beamwise direction ( $<2 \text{ cm}$ ), indicating that the effects of phase decoherence should be negligible.
- <sup>27</sup>N. C. Nguyen, J. Peraire, and B. Cockburn, "An implicit high-order hybridizable discontinuous Galerkin method for nonlinear convection diffusion equations," *J. Comput. Phys.* **228**, 8841–8855 (2009).
- <sup>28</sup>R. Ono and T. Oda, "Formation and structure of primary and secondary streamers in positive pulsed corona discharge—effect of oxygen concentration and applied voltage," *J. Phys. D* **36**, 1952 (2003).
- <sup>29</sup>E. W. McDaniel and E. A. Mason, *The Mobility and Diffusion of Ions in Gases* (Wiley, New York, 1973).